J Math Chem (2013) 51:2033–2061
DOI 10.1007/s10910-013-0198-8

ORIGINAL PAPER

Closed form analytical approach for a second order non-linear ODE interpreting EPDM vulcanization with peroxides

G. Milani

Received: 6 February 2013 / Accepted: 23 May 2013 / Published online: 6 June 2013

Abstract In this paper, the recently presented kinetic model proposed in Milani and Milani (J Math Chem 51(3):1116–1133, 2013) to interpret EPDM peroxide vulcanization is extensively revised and the resultant second order ODE is solved by means of an approximate but effective closed form analytical approach. The model has kinetic base and it is aimed at predicting, by means of a very refined approach, the vulcanization degree of rubber vulcanized with peroxides. Such a procedure takes contemporarily into consideration, albeit within a simplified scheme, the actual reactions occurring during peroxidic curing, namely initiation, H-abstraction, combination and addition, and supersedes the simplified approach used in practice, which assumes for peroxidic curing a single first order reaction. The main drawback of the overall procedure proposed in Milani and Milani (J Math Chem 51(3):1116–1133, 2013) is that the single second order non-linear differential equation obtained mathematically and representing the crosslink evolution with respect to time, was solved numerically by means of a Runge–Kutta approach. Such a limitation is here superseded and a major improvement is proposed allowing the utilization of an approximate but still effective closed form solution. After some simplifications applied on some parts of the solving function not allowing direct closed form integration, an analytical function is proposed. Kinetic parameters within the analytical model are evaluated through least squares where target data are represented by few experimental normalized rheometer curve values. In order to have an insight into the reliability of the numerical approach proposed, a case of technical interest of an EPDM with low unsaturation and crosslinked with three different peroxides at three increasing temperatures is critically discussed.

G. Milani (✉)
Politecnico di Milano, Piazza Leonardo da Vinci 32, 20133 Milano, Italy
e-mail: gabriele.milani@polimi.it

Keywords Vulcanization · Peroxides · Mathematical model · Second order differential equation · Closed form solution

1 Introduction

The subject of peroxide curing has always been of interest to chemists and physicists working in the elastomer field, see e.g. [1–6]. The reasons for this interest stem mainly from the relatively simple chemistry involved and the simple resulting network structure. The more widely used vulcanization systems based upon sulphur or sulphur compounds are very much more complex in mechanism and produce more varied crosslinks [7–13] together with other chain modifications.

At present, it can be stated that a huge amount of both experimental investigations and numerical models for EPDM cured with peroxides is available in the technical literature. However, the determination of the exact chemistry of vulcanization as well as the identification of the partial reactions occurring during curing, are still an open issue.

Recently, basing on the research carried on by van Duin and co-workers in [14–19] aimed at identifying more precisely the chemical mechanisms of peroxide curing, Milani and Milani [1] proposed a relatively simple mathematical differential model aimed at evaluating numerically the degree of crosslink of EPDM subjected to peroxide curing. The approach bases on the actual reactions occurring in practice, namely initiation with thermal decomposition of the peroxide, abstraction of H-atoms from the EPDM polymer and formation of EPDM macro-radicals (EPDM•), combination and addition.

After suitable algebraic computations on the system of first order differential equations derived from the actual chemistry of reaction, a second order non linear and non homogeneous differential equation was obtained in [1], called hereafter 2ODENL for the sake of brevity. In general, it is not possible to solve 2ODENL in closed form. Therefore, in [1], a standard Runge–Kutta numerical approach was adopted.

Subsequently, a least squares best fitting of 2ODENL solution on normalized rheometer experimental data was performed to evaluate partial reaction kinetic constants. It can be shown that such last optimization is numerically quite inexpensive, because it is generally performed on a few experimental values (10–20 points on the rheometer curves are sufficient to obtained very reliable approximations of the actual experimental behavior). In addition, it is very stable and requires a few iterations for a satisfactory convergence.

On the contrary, the utilization of a standard Runge–Kutta algorithm is quite cumbersome, because a new system of first order differential equations has to be written starting from 2ODENL, this last approach being in contradiction with the original aim of the mathematical model proposed in [1], i.e. to avoid the numerical solution of the original multi-variable first order differential equation system deduced from the chemistry of reaction. In addition, since kinetic constants are unknown, the aforementioned Runge–Kutta approach has to be embedded within the least squares optimization procedure, thus requiring a new expensive computation for each iteration within the optimization procedure adopted.

In order to eliminate this major drawback of the numerical procedure proposed in [1], in the present paper, a closed form analytical solution for 2ODENL is found. Such a solution contains, however, an infinite integral term, which unfortunately cannot be integrated in closed form. For this reason, an approximating function allowing explicit integration is found, assuming to minimize the gap between the original and approximating functions on the integration domain.

In this way, a relatively simple approximated expression for EPDM crosslink density as a function of curing time is proposed.

Kinetic parameters within the analytical model are again evaluated through least squares where target data are represented by few experimental normalized rheometer curve values.

In order to have an insight into the reliability of the numerical approach proposed, also in comparison with the numerical approach presented in [1], a case of technical interest of an EPDM with low unsaturation and crosslinked with three different peroxides at three increasing temperatures is critically discussed.

2 The kinetic mathematical model proposed

Some probable mechanism of EPM/EPDM peroxide curing and the structures formed have been recently reviewed by van Duin and co-workers in [14–19].

The complex set of the reactions that characterize peroxide cross-linking involves homolytic cleavage of peroxide, oxy and alkyl radicals, hydrogen abstraction, radical coupling (cross-link formation), polymer scission and radical transfer. In the case of EPDM, the amount and type of the third-monomer, are also important parameters to consider, but they can be safely disregarded in a first approximation of the phenomenon for those EPDMs having lower concentrations of the third-monomer. From an experimental viewpoint, the precise structure of the various products could be obtained either by an interpretation of the mass spectrometry data or by means of a solid state ^{13}C nuclear magnetic resonance (NMR) study, as done in [19], where it is shown that an increase in sensitivity is achieved.

The generally accepted basic chemistry [14–19] of EPDM vulcanized with peroxides is the following:

$$\begin{array}{ll}
\frac{1}{2}\mathrm{ROOR} \rightarrow \mathrm{RO}\bullet \rightarrow \mathrm{R}'\bullet & \text{initiation} \\
\mathrm{EP(D)M\text{-}H} + \mathrm{RO}\bullet/\mathrm{R}'\bullet \rightarrow \mathrm{EP(D)M}\bullet + \mathrm{ROH}/\mathrm{R}'\mathrm{H} & \text{H-abstraction} \\
2\mathrm{EP(D)M}\bullet \rightarrow \mathrm{EP(D)M\text{-}EP(D)M} & \text{combination} \\
\mathrm{EP(D)M}\bullet + \mathrm{EP(D)M} \rightarrow \mathrm{EP(D)M} - \mathrm{EP(D)M}\bullet \rightarrow \mathrm{EP(D)M} - \mathrm{EP(D)M} - \mathrm{H} & \text{addition}
\end{array} \tag{1}$$

The chain of free-radical reactions is initiated by thermal decomposition of the peroxide, yielding primary alkoxy (RO•) or secondary alkyl radicals (R′•). Subsequent abstraction of H-atoms from the EPDM polymer results in the formation of EPDM macro-radicals (EPDM•). Calculations based on kinetic data for H-abstraction indicate that H-abstraction mainly occurs along the saturated EPM polymer backbone

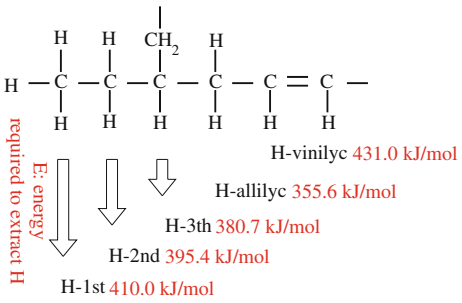

Fig. 1 Energy required in order to extract hydrogen atom from the backbone of the macromolecules at 0 K. At 25 °C add 1 Kcal

[20], whereas several electron paramagnetic resonance (EPR) spectroscopy studies have shown the selective formation of allyl radicals derived from the diene monomer.

Considering the energy required for the abstraction of the H-atoms, see Fig. 1, within the formation of the back-bone, the allyl radicals are more probable than the others, because of the lowest energy required by the abstraction of the H-atoms.

The actual cross-linking proceeds through two pathways, which have been shown to be additive [21]. Two EPDM macro-radicals either combine or, alternatively, a macro-radical adds to an EPDM unsaturation. Visible spectroscopy has confirmed the conversion of the EPDM unsaturation upon peroxide cure [14–25]. It is noted that in practical EPDM/peroxide compounds, usually co-agents, such as triallyl (iso)cyanurate, trimethylolpropane trimethacrylate or m-phenylenebis(maleimide), are included to increase the peroxide curing efficiency [16], which obviously affects the mechanism of peroxide cure.

Adopting for EPDM the kinetic scheme constituted by the chemical reactions summarized in Eq. (1) and already adopted by other authors see e.g. [21,25], in [1] differential mathematical relations among chemical quantities involved in the reticulation process (1) were deduced. In particular, the chemical reactions appearing in (1) may be schematized as follows:

$$\begin{aligned} I &\xrightarrow{k_1} 2R \\ R + P &\xrightarrow{k_2} P^* \\ 2P^* &\xrightarrow{k_3} P_r^* \\ P^* &\xrightarrow{k_4} P_i^* \end{aligned} \tag{2}$$

In Eq. (2), I is the peroxide, R the primary alkoxy (RO•) or secondary alkyl radicals (R′•), P the uncured polymer, P^* is the EPDM macro-radical, P_r^* and P_i^* the matured cross-linked polymers, and $K_{1,\ldots,4}$ are kinetic reaction constants. Here it is worth emphasizing that $K_{1,\ldots,4}$ are temperature dependent quantities, hence they rigorously should be indicated as $K_{1,\ldots,4}(T)$, where T is the absolute temperature. In what follows, for the sake of simplicity, the temperature dependence will be left out.

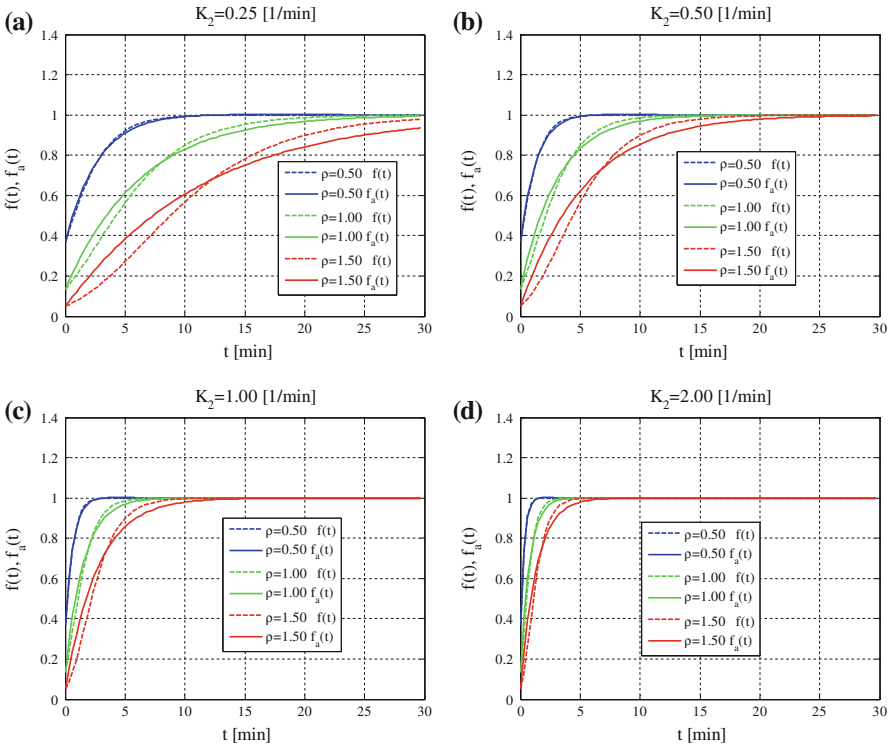

Fig. 2 Functions $f(t)$ and $f_a(t)$ at different ρ and K_2 values. **a** $K_2 = 0.25$ (1/min). **b** $K_2 = 0.50$ (1/min). **c** $K_2 = 1.00$ (1/min). **d** $K_2 = 2.00$ (1/min)

By means of the so called xyz method, independent variables may be established. From stoichiometry of the reaction, it can be argued that:

$$\begin{aligned} I &= I_0 - x \\ R &= 2x - y \\ P &= P_0 - y \\ P^* &= y - 2z - q \\ P_r^* &= z \\ P_i^* &= q \end{aligned} \tag{3}$$

Obviously, from (3) it can be also deduced that independent variables are $I(t)$, $R(t)$, $P_r^*(t)$ and $P_i^*(t)$. Indeed, from (3) it turns out that:

$$\begin{aligned} x &= I - I_0 \\ y &= 2(I - I_0) - R \\ P &= P_0 + R - 2(I - I_0) \\ P^* &= 2(I - I_0) - R - 2P_r^* - P_i^* \end{aligned}$$

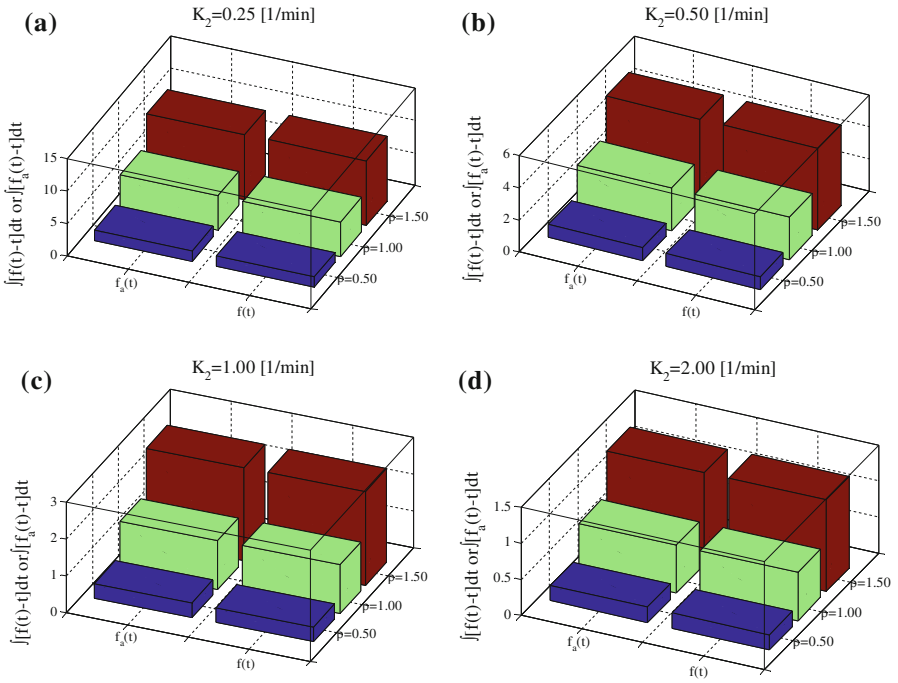

Fig. 3 Evaluation of $\int_0^{+\infty}[f(t)-t]dt$ and $\int_0^{+\infty}[fa(t)-t]dt$ at different ρ and K_2 values. **a** $K_2 = 0.25$ (1/min). **b** $K_2 = 0.50$ (1/min). **c** $K_2 = 1.00$ (1/min). **d** $K_2 = 2.00$ (1/min)

$$z = P_r^*$$
$$q = P_i^* \tag{4}$$

The aim is to provide an analytical expression for vulcanized rubber, i.e. concentration of P^* with respect to time.

From (2) and (3) and well established kinetic rules, the following set of differential equations may be written:

$$\text{(a)}\ \frac{dI}{dt} = -K_1 I$$
$$\text{(b)}\ \frac{dR}{dt} = 2K_1 I - K_2 RP$$
$$\text{(c)}\ \frac{dP}{dt} = -K_2 RP$$
$$\text{(d)}\ \frac{dP^*}{dt} = K_2 RP - K_3 \left(P^*\right)^2 - K_4 P^*$$
$$\text{(e)}\ \frac{dP_r^*}{dt} = K_3 \left(P^*\right)^2$$
$$\text{(f)}\ \frac{dP_i^*}{dt} = K_4 P^* \tag{5}$$

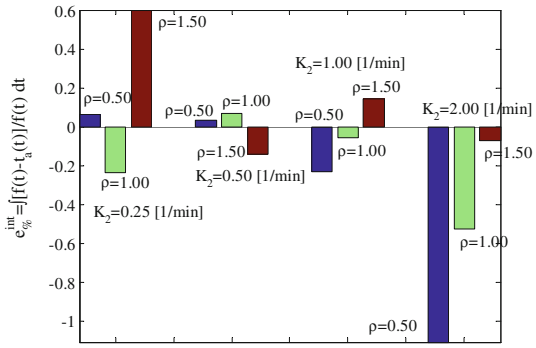

Fig. 4 Evaluation of relative error $e_{\%}^{\text{int}} = 100 \int_0^{+\infty} \frac{[f(t)-f_a(t)]}{f(t)} dt$ at different ρ and K_2 values

Equation (5)a may be solved immediately by separation of variables, allowing to determine the concentration of peroxide with respect to time:

$$I = I_0 e^{-K_1(t-t_0)} \tag{6}$$

From (6) and performing the difference between Eqs. b and c in (5) we obtain:

$$\frac{dR}{dt} - \frac{dP}{dt} = 2K_1 I = 2K_1 I_0 e^{-K_1(t-t_0)} \tag{7}$$

Differentiating Eq. (5)c, it turns out that:

$$\frac{d^2P}{dt^2} = -K_2 R \frac{dP}{dt} - K_2 P \frac{dR}{dt} \tag{8}$$

From (7), remembering from (5) that $R = -\frac{1}{K_2 P}\frac{dP}{dt}$, the second order differential Eq. (8) may be re-written exclusively in terms of P as follows:

$$\frac{d^2P}{dt^2} - \frac{1}{P}\left(\frac{dP}{dt}\right)^2 + K_2 P \frac{dP}{dt} + 2K_1 K_2 I_0 P e^{-K_1(t-t_o)} = 0 \tag{9}$$

Equation (9) is a non-linear and non-homogeneous second order differential equation in the sole variable P.

Assuming $t_0 = 0$, Eq. (9) simplifies into:

$$\frac{d^2P}{dt^2} - \frac{1}{P}\left(\frac{dP}{dt}\right)^2 + K_2 P \frac{dP}{dt} + 2K_1 K_2 I_0 P e^{-K_1 t} = 0 \quad \text{(2ODENL)} \tag{10}$$

ODE (10), labeled hereafter as 2ODENL, has been found in [1], where a numerical Runge–Kutta approach was used to find an approximation of the solution.

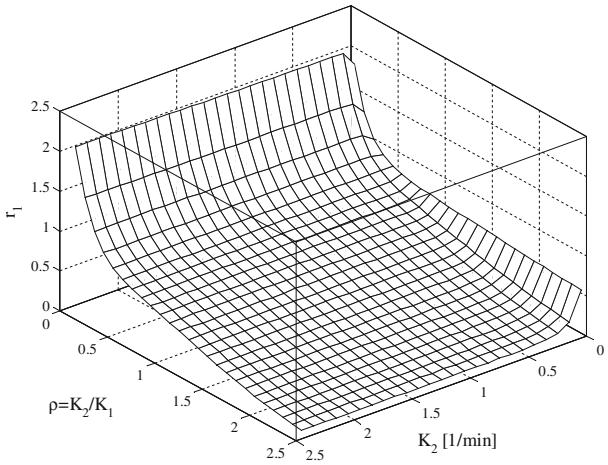

Fig. 5 Numerical evaluation of parameter r_1 as a function of ρ and K_2 variables

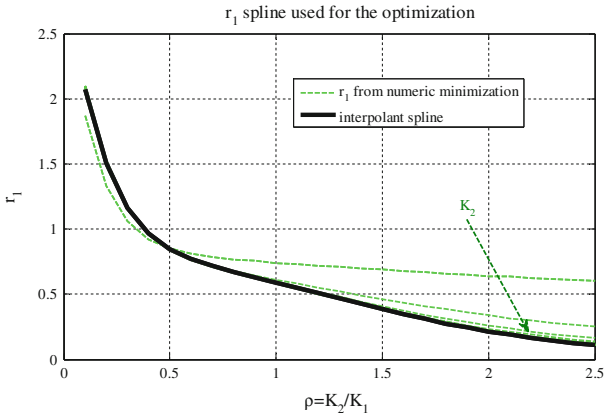

Fig. 6 Spline interpolation of parameter r_1 as a function of ρ variable only

Indeed, it has to be emphasized that the determination of a closed form solution for 2ODENL is not an easy task. However, it can be shown that the following function:

$$P(t) = \frac{e^{\left(C_1 t - \frac{2K_2}{K_1 e^{K_1 t}}\right)}}{C_2 + \int K_2 e^{\left(C_1 t - \frac{2K_2}{K_1 e^{K_1 t}}\right)} dt} \tag{11}$$

satisfies ODE (10), where C_1 and C_2 are constants to be determined basing on boundary conditions.

It can be proved that (11) is the solution of (10) by inverse substitution. Indeed, let us assume the following simplified symbolic representation of P and its derivatives:

Table 1 Experimental data set analyzed, EPDM without reversion, composition in phr

Polymer	VISTALON 1703P Ethylene in wt.%76.2 VNB-vinylnorbornene in wt.%0.9 Mooney ML (1 + 4) 100 °C 35.3 Manufacturer (Exxon)	54
Silane treated calcinated kaolin		30
Antioxidants		8
LDPE Riblene MR 10 MFI = 18.7 (ASTM D1238)		6
PE WAX		1
Peroxide		1

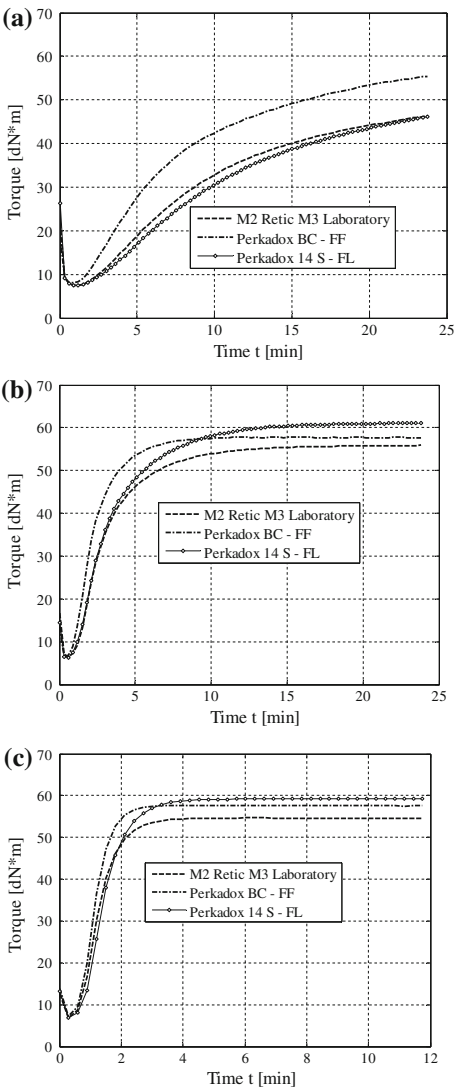

Fig. 7 Experimental torque curves used in the numerical simulations. **a** 160 °C. **b** 180 °C. **c** 200 °C

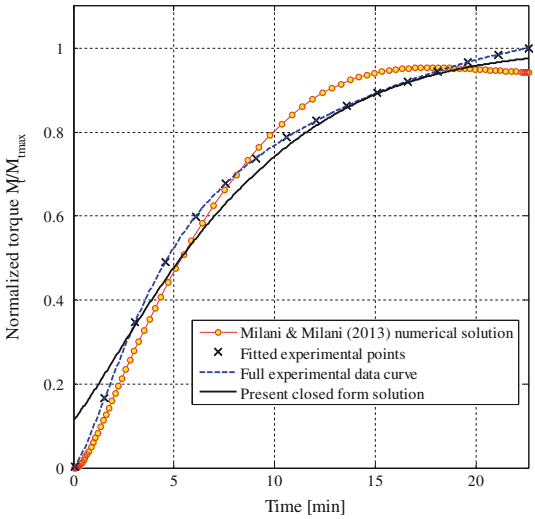

Fig. 8 EPDM vulcanized with Perkadox BC-FF, 160 °C. Comparison among experimental data, previously presented numerical approach and present closed form solution

$$P = \frac{g_3(x)}{g_0(x)}\frac{dP}{dt} = \frac{\left(C_1 + \frac{2K_2}{e^{K_1 t}}\right) e^{\left(C_1 t - \frac{2K_2}{K_1 e^{K_1 t}}\right)}}{g_0(x)} - \frac{K_2 e^{2C_1 t - \frac{4K_2}{K_1 e^{K_1 t}}}}{[g_0(x)]^2}$$
$$= \frac{g_2(x)\, g_3(x)}{g_0(x)} - \frac{K_2 g_1(x)}{[g_0(x)]^2} = \frac{g_2(x)\, g_3(x)}{g_0(x)} - \frac{K_2 [g_3(x)]^2}{[g_0(x)]^2}$$

$$\frac{d^2P}{dt^2} = \frac{g_3(x)[g_2(x)]^2}{g_0(x)} - \frac{2K_1K_2g_3(x)}{g_0(x)\, e^{K_1 t}} - \frac{K_2 g_1(x)\, g_2(x)}{[g_0(x)]^2} - \frac{K_2 g_1(x)\left(2C_1 + \frac{4K_2}{e^{K_1 t}}\right)}{[g_0(x)]^2}$$
$$+ \frac{2K_2^2 g_3(x)\, g_1(x)}{[g_0(x)]^3} = \frac{g_3(x)[g_2(x)]^2}{g_0(x)} - \frac{2K_1K_2g_3(x)}{g_0(x)\, e^{K_1 t}} - \frac{K_2[g_3(x)]^2 g_2(x)}{[g_0(x)]^2}$$
$$- \frac{2K_2[g_3(x)]^2 g_2(x)}{[g_0(x)]^2} + \frac{2K_2^2[g_3(x)]^3}{[g_0(x)]^3} = \frac{g_3(x)[g_2(x)]^2}{g_0(x)} - \frac{2K_1K_2g_3(x)}{g_0(x)\, e^{K_1 t}}$$
$$- \frac{3K_2[g_3(x)]^2 g_2(x)}{[g_0(x)]^2} + \frac{2K_2^2[g_3(x)]^3}{[g_0(x)]^3} \tag{12}$$

Having defined:

$$g_0(x) = C_2 + \int K_2 e^{\left(C_1 t - \frac{2K_2}{K_1 e^{K_1 t}}\right)} dt$$
$$g_1(x) = e^{2C_1 t - \frac{4K_2}{K_1 e^{K_1 t}}} = g_3(x)^2$$
$$g_2(x) = C_1 + \frac{2K_2}{e^{K_1 t}}$$
$$g_3(x) = e^{C_1 t - \frac{2K_2}{K_1 e^{K_1 t}}} \tag{13}$$

Substituting (12) into (10), 2ODENL under study can be re-written as:

$$\frac{g_3(x)[g_2(x)]^2}{g_0(x)} - \frac{2K_1K_2g_3(x)}{g_0(x)e^{K_1t}} - \frac{3K_2[g_3(x)]^2 g_2(x)}{[g_0(x)]^2} + \frac{2K_2^2[g_3(x)]^3}{[g_0(x)]^3} + -\frac{g_0(x)}{g_3(x)}\left\{\frac{[g_2(x)]^2[g_3(x)]^2}{[g_0(x)]^2} + \frac{K_2^2[g_3(x)]^4}{[g_0(x)]^4} - 2K_2\frac{[g_2(x)][g_3(x)]^3}{[g_0(x)]^3}\right\} + +K_2\frac{g_3(x)}{g_0(x)}\left\{\frac{g_2(x)g_3(x)}{g_0(x)} - \frac{K_2[g_3(x)]^2}{[g_0(x)]^2}\right\} + \frac{2K_1K_2g_3(x)}{g_0(x)e^{K_1t}} = 0 \quad (14)$$

and hence:

$$\frac{g_3(x)[g_2(x)]^2}{g_0(x)} + \frac{(-3K_2+2K_2+K_2)[g_3(x)]^2 g_2(x)}{[g_0(x)]^2} + \frac{(2K_2^2-K_2^2-K_2^2)[g_3(x)]^3}{[g_0(x)]^3} + -\frac{g_0(x)}{g_3(x)}\left\{\frac{[g_2(x)]^2[g_3(x)]^2}{[g_0(x)]^2}\right\} - \frac{2K_1K_2g_3(x)}{g_0(x)e^{K_1t}} + \frac{2K_1K_2g_3(x)}{g_0(x)e^{K_1t}} = 0 \quad (15)$$

(15) demonstrates that (11) is the solution of 2ODENL (10).

A closed form integral for the function $\bar{f}(t) = K_2 e^{(C_1 t - \frac{2K_2}{K_1 e^{K_1 t}})}$ does not exist. Therefore, an approximant function is needed. It is worth noting that a good approximation for $\bar{f}(t)$ is the following:

$$\tilde{f}(t) = K_2 e^{C_1 t}\left[1 - e^{-\xi K_2 t} + e^{-\left(\frac{2K_2}{K_1}+K_2 t\right)}\right] \quad (16)$$

where $\xi > 0$ is a tuning parameter that allows the best fitting of the original function. In particular, it is worth noting that $\lim_{t\to+\infty}\tilde{f}(t) = \lim_{t\to+\infty}\bar{f}(t) = K_2 e^{C_1 t}$ and $\tilde{f}(0) = \bar{f}(0) = K_2 e^{-2\frac{K_2}{K_1}}$.

To properly determine ξ, we assume that $\tilde{f}(t)$ and $\bar{f}(t)$ have first derivatives in the origin with a fixed ratio $\frac{d\tilde{f}(t)}{d\bar{f}(t)} = r_1$, i.e.:

$$\frac{d\tilde{f}(t)}{dt} = K_2C_1e^{C_1t}\left[1 - e^{-\xi K_2 t} + e^{-\left(\frac{2K_2}{K_1}+K_2t\right)} + \frac{\xi K_2}{C_1} - \frac{K_2}{C_1}e^{-\left(\frac{2K_2}{K_1}+K_2t\right)}\right]_{t=0}$$
$$= K_2C_1\left[e^{-\left(\frac{2K_2}{K_1}\right)} + \frac{\xi K_2}{C_1} - \frac{K_2}{C_1}e^{-\left(\frac{2K_2}{K_1}\right)}\right] = K_2\left[C_1e^{-\left(\frac{2K_2}{K_1}\right)} + \xi K_2 - K_2e^{-\left(\frac{2K_2}{K_1}\right)}\right]$$

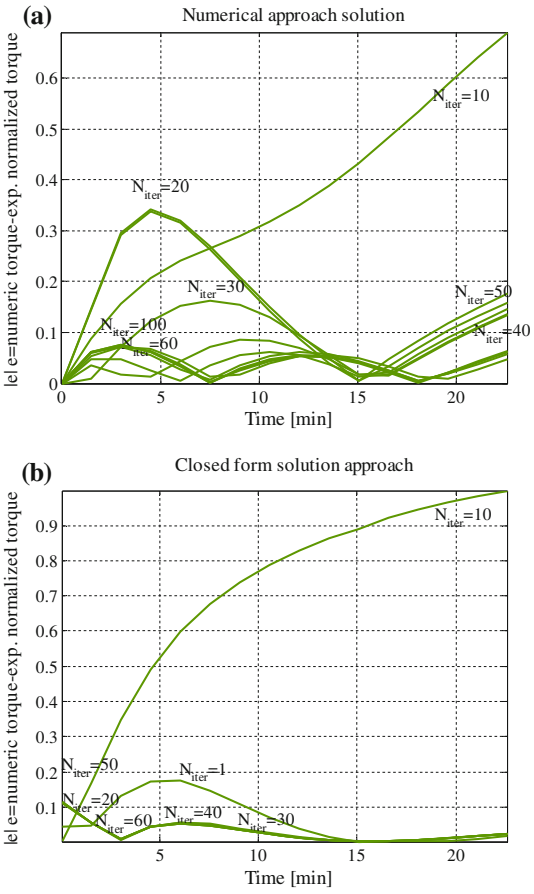

Fig. 9 EPDM vulcanized with Perkadox BC-FF, 160 °C. Absolute error charts at successive iterations. **a** Previously presented numerical approach. **b** Present closed form solution

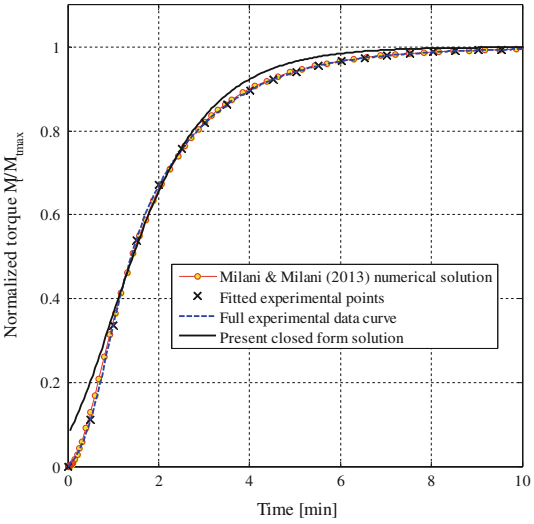

Fig. 10 EPDM vulcanized with Perkadox BC-FF, 180 °C. Comparison among experimental data, previously presented numerical approach and present closed form solution

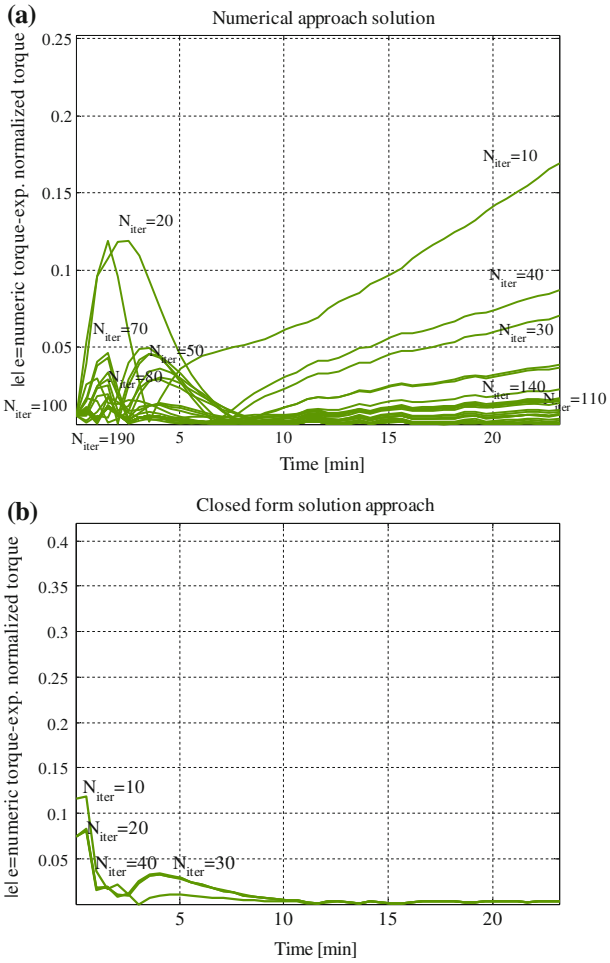

Fig. 11 EPDM vulcanized with Perkadox BC-FF, 180 °C. Absolute error charts at successive iterations. **a** Previously presented numerical approach. **b** Present closed form solution

$$= K_2^2\left[\left(\frac{C_1}{K_2}-1\right)e^{-2\rho}+\xi\right]\frac{d\bar{f}(t)}{dt} = \left[K_2\left(C_1+\frac{2K_2}{e^{K_1 t}}\right)e^{\left(C_1 t-\frac{2K_2}{K_1 e^{K_1 t}}\right)}\right]_{t=0}$$
$$= K_2^2\left(\frac{C_1}{K_2}+2\right)e^{-2\rho} = r_1\frac{d\tilde{f}(t)}{dt} \tag{17}$$

where we have indicated with ρ the ratio between K_2 and K_1.

Equating the two derivatives in (17) and taking into account the coefficient r_1 we obtain:

$$\xi = \left[\frac{C_1}{K_2}\left(\frac{1}{r_1}-1\right)+\frac{2}{r_1}+1\right]e^{-2\rho} \tag{18}$$

It is interesting to notice that (18) does not depend on C_1 and C_2 if $r_1 = 1$. The choice of r_1 is iterative, as it will be demonstrated hereafter and is aimed at minimizing the differences between integrals in Eq. (11) provided by functions $\bar{f}(t)$ and $\tilde{f}(t)$. Results of the numerical minimization, see after, should be provided either in tabular or graphical form, varying K_2 and ρ parameters.

It is also interesting to notice that (18) depends exclusively on ρ ratio.

It is also possible to compare functions $\tilde{f}(t)$ and $\bar{f}(t)$ once constants C_1 and C_2 are known, for an a-posteriori evaluation of the effectiveness of the approximation adopted.

Substituting $\bar{f}(t)$ with $\tilde{f}(t)$ into the solution (11) of the ODE Eq. (10), it is possible to explicitly integrate the indefinite integral appearing on (11), namely:

$$\begin{aligned} P(t) &= \frac{e^{\left(C_1 t - \frac{2K_2}{K_1 e^{K_1 t}}\right)}}{C_2 + \int K_2 e^{\left(C_1 t - \frac{2K_2}{K_1 e^{K_1 t}}\right)} dt} \cong \frac{e^{\left(C_1 t - \frac{2K_2}{K_1 e^{K_1 t}}\right)}}{C_2 + \int K_2 e^{C_1 t}\left[1 - e^{-\xi K_2 t} + e^{-\left(\frac{2K_2}{K_1} + K_2 t\right)}\right] dt} \\ &= \frac{e^{\left(C_1 t - \frac{2K_2}{K_1 e^{K_1 t}}\right)}}{\tilde{C}_2 + \frac{K_2}{C_1} e^{C_1 t} - \frac{K_2}{C_1 - \xi K_2} e^{(C_1 - \xi K_2)t} + \frac{K_2}{C_1 - K_2} e^{(C_1 - K_2)t - \frac{2K_2}{K_1}}} \\ &= \frac{e^{C_1 t} e^{-2\frac{\rho}{e^{K_1 t}}}}{\tilde{C}_2 + \frac{K_2}{C_1} e^{C_1 t} - \frac{K_2}{C_1 - \xi K_2} e^{C_1 t} e^{-\xi K_2 t} + \frac{K_2}{C_1 - K_2} e^{C_1 t} e^{-K_2 t} e^{-2\rho}} \end{aligned} \tag{19}$$

Having indicated with $\tilde{C}_2 = C_2 + C_3$, and with C_3 an additional integration constant of the indefinite integral.

It is interesting to notice from (19) that:

$$\lim_{t \to +\infty} P(t) = \frac{e^{C_1 t}}{e^{C_1 t}\left(\frac{K_2}{C_1} - \frac{K_2}{C_1 - \xi K_2} e^{-\xi K_2 t} + \frac{K_2}{C_1 - K_2} e^{-K_2 t} e^{-2\rho}\right)} = \frac{K_2}{C_1} \tag{20}$$

Since Eq. (9) holds for vulcanization without reversion, $\lim_{t \to +\infty} P(t) = 1$. As a consequence, from (20) we obtain:

$$\lim_{t \to +\infty} P(t) = 1 \Leftrightarrow C_1 = K_2 \tag{21}$$

By means of Eq. (21) and Eq. (18), we can re-write $\tilde{f}(t)$ as:

$$\begin{aligned} \tilde{f}(t) &= K_2 e^{K_2 t}\left[1 - e^{-\xi K_2 t} + e^{-(2\rho + K_2 t)}\right] \\ &= K_2\left[e^{K_2 t} - e^{\left(1 - \frac{3}{r_1} e^{-2\rho}\right) K_2 t} + e^{-(2\rho)}\right] \\ &= K_2 e^{K_2 t}\left[1 - e^{-\frac{3}{r_1} e^{-2\rho} K_2 t} + e^{-(2\rho + K_2 t)}\right] \end{aligned} \tag{22}$$

In Fig. 2, functions $f(t) = \bar{f}(t)/(K_2 e^{K_2 t})$ and $f_a(t) = \tilde{f}(t)/(K_2 e^{K_2 t})$ are compared in correspondence of four values of K_2 (respectively equal to 0.25, 0.5, 1 and 2), at three different ρ ratios. As it is possible to notice, the approximation is quite satisfactory for all the cases inspected, meaning that the substitution adopted in (19) is adequate.

In Fig. 3, the two definite integrals $\int_0^{+\infty}[f(t)-t]dt$ and $\int_0^{+\infty}[f_a(t)-t]dt$ are evaluated at different ρ and K_2 values. Such representation provides a visual estimate of the difference between $f(t)$ and $f_a(t)$ in integral form (subtracting t to obtain a definite integral), i.e. demonstrate the correctness of the approximation for the declared purposes. As it is possible to notice indeed, for all the cases inspected, $\int_0^{+\infty}[f(t)-t]dt$ and $\int_0^{+\infty}[f_a(t)-t]dt$ are very similar.

The goodness of the approximation is also demonstrated by the relative error function on integrals shown in Fig. 3 and depicted in Fig. 4, where the relative error $e^{\text{int}}_{\%}$, defined as $100\int_0^{+\infty}\frac{[f(t)-f_a(t)]}{f(t)}dt$, is evaluated at different ρ and K_2 values.

Values of the coefficient r_1 are preliminarily evaluated solving the following minimization problem, at fixed K_2 and ρ parameters:

$$\begin{aligned} \min_{r_2}\Omega(\xi) &= \min\int_0^{+\infty}\left|1-\frac{\bar{f}(t)}{\tilde{f}(t)}\right|dt \\ \xi &= \frac{3}{r_1}e^{-2\rho} \\ \rho, K_2 &\equiv \text{ assigned parameters} \end{aligned} \tag{23}$$

It is interesting to notice that, while functions $\bar{f}(t)$ and $\tilde{f}(t)$ tend asymptotically to $K_2 e^{K_2 t}$ for large values of t, we obtain:

$$\lim_{t\to+\infty}\left|1-\frac{\bar{f}(t)}{\tilde{f}(t)}\right| = \lim_{t\to+\infty}\left|1-\frac{e^{\left(-2\rho e^{-K_1 t}\right)}}{1-e^{-\frac{3}{r_1}e^{-2\rho}K_2 t}+e^{-(2\rho+K_2 t)}}\right| = 0 \tag{24}$$

The integral entering into optimization problem (23) is definite and allows the determination of r_1 numerically.

Usually, K_2 and K_1 may range between 0.1 and 5 (unit of measure: 1/min), with ρ ranging from 0.25 to 2. Values of the parameter r_1 found through the minimization problem (23) are sketched in Fig. 5 as a function of K_2 and ρ variables.

As can be noted from Fig. 5, r_1 exhibits little variability with K_2. As a consequence, it is reasonable to evaluate coefficients of an interpolating spline having as independent variable ρ.

Results are represented in Fig. 6 with a comparison with functions from minimization problem (23) at fixed K_2.

Assuming $C_1 = K_2$, the last integral of $\tilde{f}(t)$ contains an infinite term, see Eq. (19). Therefore $\tilde{f}(t)$ has to be re-written as in (22) and re-integrated to provide again

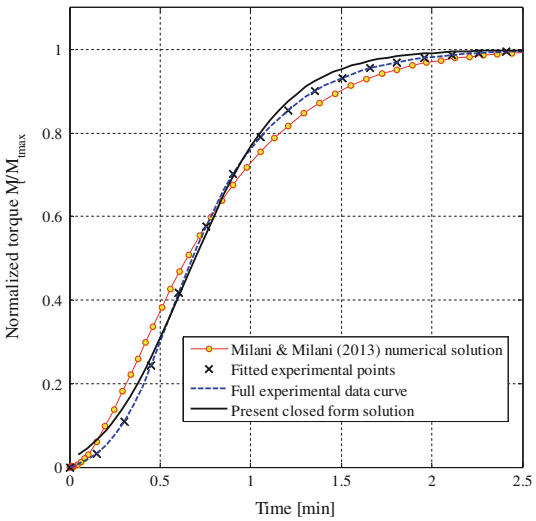

Fig. 12 EPDM vulcanized with Perkadox BC-FF, 200 °C. Comparison among experimental data, previously presented numerical approach and present closed form solution

function $P(t)$ as:

$$\begin{aligned} P(t) &= \frac{e^{\left(C_1 t - \frac{2K_2}{K_1 e^{K_1 t}}\right)}}{C_2 + \int K_2 \left(e^{K_2 t} - e^{K_2(1-\xi)t} + e^{-2\rho}\right) dt} \\ &= \frac{e^{\left(K_2 t - \frac{2K_2}{K_1 e^{K_1 t}}\right)}}{\tilde{C}_2 + e^{K_2 t} - K_2 \frac{1}{1-\xi} e^{K_2(1-\xi)t} + e^{-2\rho} t} \\ &= \frac{e^{K_2 t} e^{-2\frac{\rho}{e^{K_1 t}}}}{\tilde{C}_2 + e^{K_2 t} - K_2 \frac{1}{1-\xi} e^{K_2(1-\xi)t} + e^{-2\rho} t} \end{aligned} \tag{25}$$

$\tilde{C}_2$ is evaluated imposing the passage, at a time t_0, of function (25) on $P(t_0)$, i.e.:

$$\tilde{C}_2 = \frac{e^{K_2 t_0} e^{-2\frac{\rho}{e^{K_1 t_0}}} - P(t_0)\left[e^{K_2 t_0} - K_2 \frac{1}{1-\xi} e^{K_2(1-\xi)t_0} + e^{-2\rho} t_0\right]}{P(t_0)} \tag{26}$$

It is interesting to notice from (25) and (26) that:

$$P(0) = \frac{e^{-2\rho}}{\frac{e^{K_2 t_0} e^{-2\frac{\rho}{e^{K_1 t_0}}} - P(t_0)\left[e^{K_2 t_0} - K_2 \frac{1}{1-\xi} e^{K_2(1-\xi)t_0} + e^{-2\rho} t_0\right]}{P(t_0)} + 1 - K_2 \frac{1}{1-\xi}} \tag{27}$$

Which generally is a number different from zero. It it therefore expected a non negligible error of the model near the origin when normalized rheometer curves after

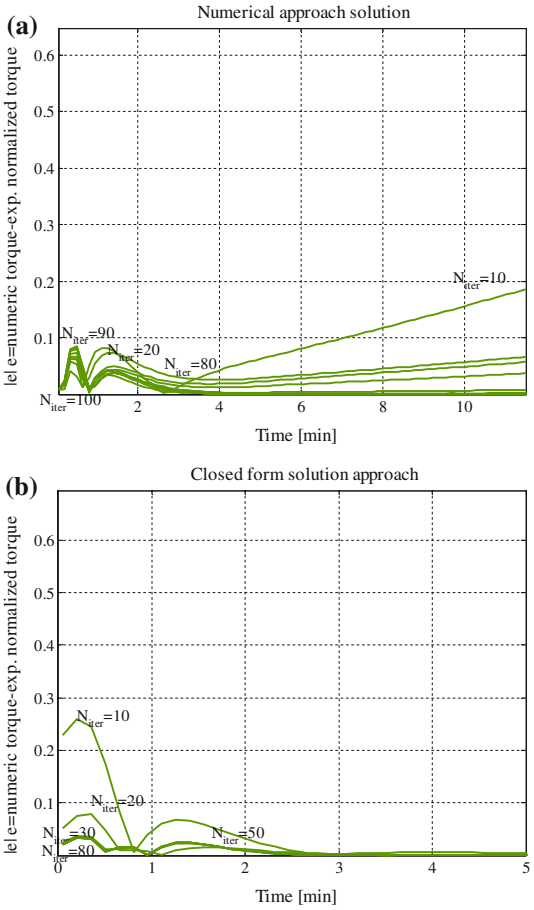

Fig. 13 EPDM vulcanized with Perkadox BC-FF, 200 °C. Absolute error charts at successive iterations. **a** Previously presented numerical approach. **b** Present closed form solution

the scorch point are used to evaluate kinetic constants. In this case, indeed, scorch point is assumed as axis origin and therefore $P(0) = 0$.

In presence of reversion, not treated here and left to a future contribution, $P(t)$ does not represent the crosslink degree. Indeed, the knowledge of P^* is required. P^* may be determined from $R(t)$. In particular, from Eq. (5)d, P^* is evaluated solving the following ODE:

$$\frac{dP^*}{dt} = K_2 R(t) P(t) - K_3 \left(P^*\right)^2 - K_4 P^* \tag{28}$$

Equation (28) is a first order non linear differential equation, which could be solved using a Runge–Kutta numerical approach [1,26].

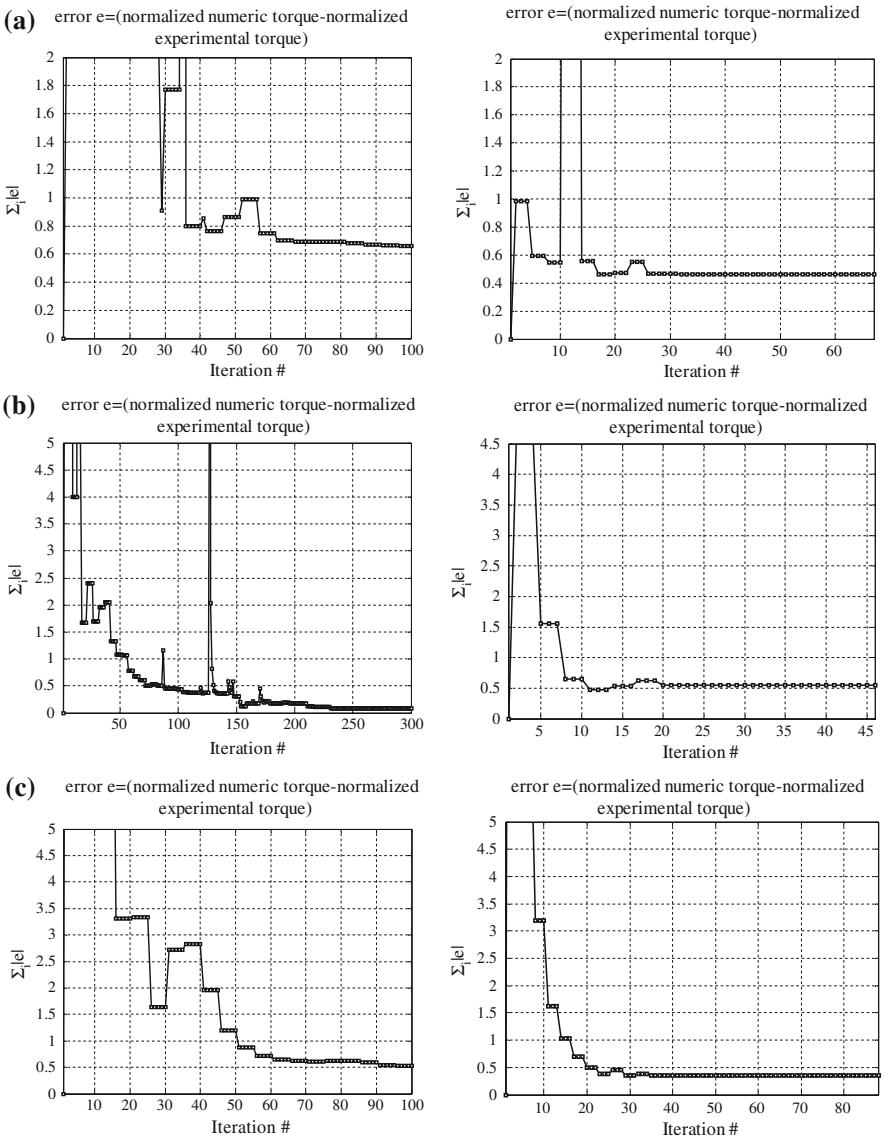

Fig. 14 EPDM vulcanized with Perkadox BC-FF. Convergence of the least squares routine assuming as target the absolute error. *Left*: numerical literature approach. *Right*: present closed form model. **a** 160 °C. **b** 180 °C. **c** 200 °C

3 Numerical applications

In order to assess the capabilities of the closed form differential equation model when compared to [1] approach in absence of reversion, an EPDM with low unsaturation level tested by the author in [27] is here considered as reference data.

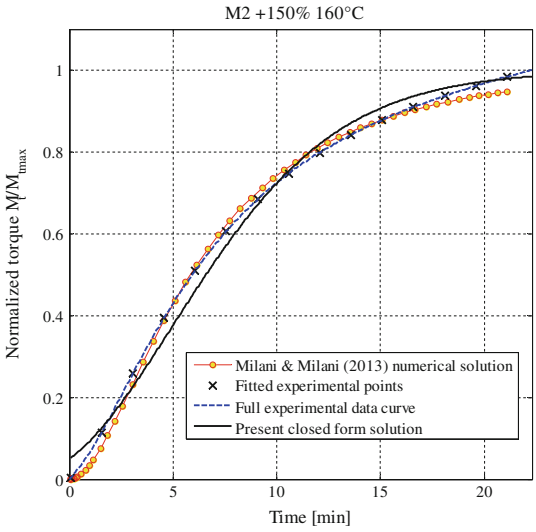

Fig. 15 EPDM vulcanized with M2 curing agent, 160 °C. Comparison among experimental data, previously presented numerical approach and present closed form solution

Attention is focused exclusively on the capabilities of the numerical approach to fit experimental evidences. The EPDM blend is vulcanized in an oscillating disc rheometer, at three different temperatures (160, 180 and 200 °C) by means of three different curing agents, namely two singles peroxides (Perkadox BC-FF and Perkadox 14S-FL, hereafter called BC-FF and 14-S) and a mixture of three peroxides (Trigonox-T, Perkadox BC-FF and Perkadox 14S-FL, hereafter called M2 for the sake of clearness). The blend under consideration has the composition schematically reported in Table 1.

The commercial names by Akzo [28] Trigonox-T, Perkadox BC-FF and Perkadox 14S-FL are respectively tert-butyl cumil peroxide, dycumil peroxide and di(tert-butylperoxyisopropyl) benzene. They exhibit a half-life time equal to 1 h at temperatures equal to 146, 138 and 146 °C, respectively. The peroxides are therefore quite similar (Trigonox-T and Perkadox 14S-FL have indeed, exactly the same behavior); nonetheless, some perceivable differences in the experimental rheometer curves of the EPDM under consideration are visible. In all cases, experimental results, as expected, do not exhibit perceivable reversion. Experimental rheometer curves are comparatively represented for the three curing agents in Fig. 7 at the three vulcanization temperatures investigated.

To perform a numerical optimization of the kinetic model proposed, experimental torque values are normalized dividing each point of the curve by the maximum torque, so that experimental data are always within the range 0–1.

The results of the numerical simulations are comparatively represented in Figs. 8, 9, 10, 11, 12, 13, 14, 15, 16, 17, 18, 19, 20, 21, 22, 23, 24, 25, 26, 27, and 28.

Numerical curves for both present and [1] approach are obtained using a non-linear least squares procedure, for which the convergence performance is evaluated and represented as follows:

- For Peroxide BC-FF in Fig. 9 at 160°, in Fig. 11 at 180 °C and in Fig. 13 at 200 °C;
- For M2 Curing agent in Fig. 16 (160 °C), Fig. 18 (180 °C) and Fig. 20 (200 °C);

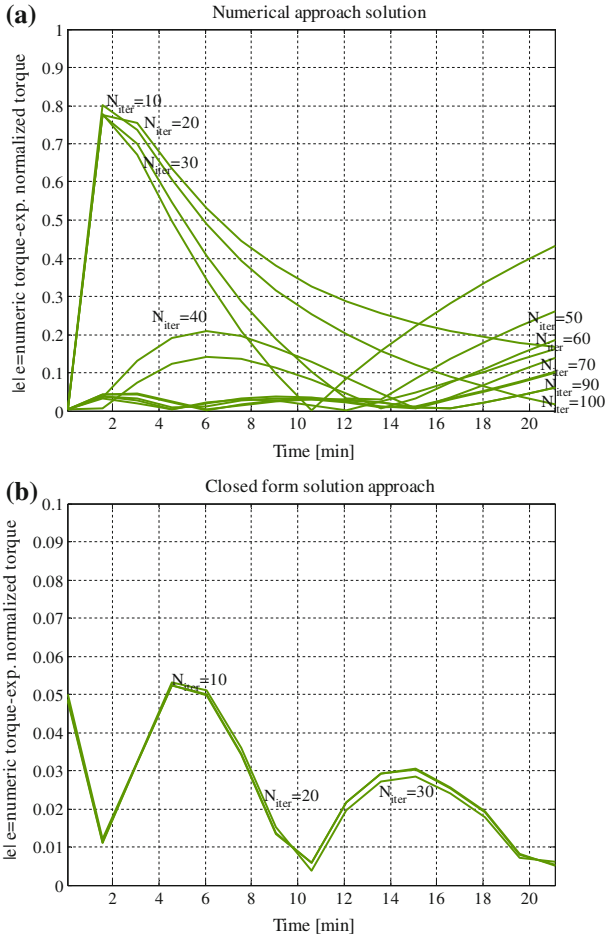

Fig. 16 EPDM vulcanized with M2 curing agent, 160 °C. Absolute error charts at successive iterations. **a** Previously presented numerical approach. **b** Present closed form solution

- For Peroxide 14-S in Fig. 23 (160 °C), Fig. 25 (180 °C) and Fig. 27 (200 °C).

In all the aforementioned figures, the absolute value |e| of the difference between numerical prediction and experimental normalized torque at successive instants (from zero to the end of vulcanization) is represented. Each curve corresponds to a least squares iteration. In subfigures—a, the convergence of model [1] is depicted, whereas in subfigures—b the performance of the present approach is reported. It is obviously expected that, for both models, curves approach zero after a sufficiently elevated number of iterations, meaning that the least squares routine is achieving convergence to the target points.

To have a further insight into the efficiency of the two compared numerical procedures, in Figs. 14, 21 and 28 the quantity $\Sigma_i |e|$ is represented at successive iterations, both for the present closed form approach (right) and the previously presented numer-

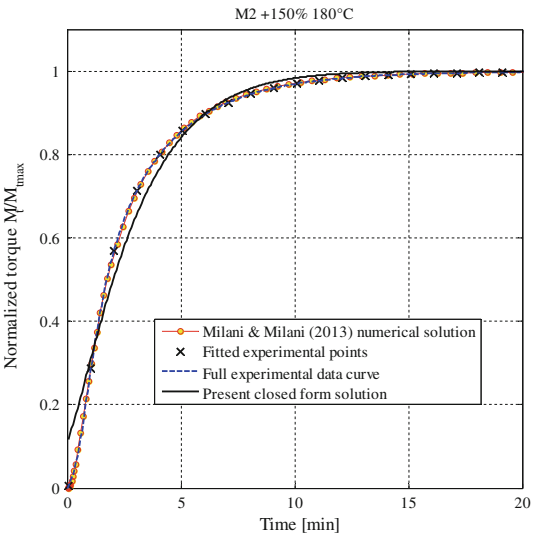

Fig. 17 EPDM vulcanized with M2 curing agent, 180 °C. Comparison among experimental data, previously presented numerical approach and present closed form solution

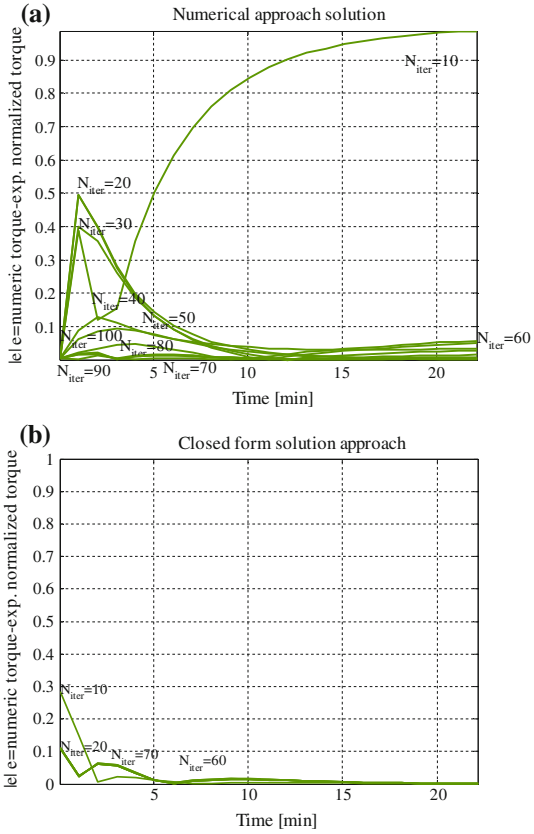

Fig. 18 EPDM vulcanized with M2 curing agent, 180°C. Absolute error charts at successive iterations. **a** Previously presented numerical approach. **b** Present closed form solution

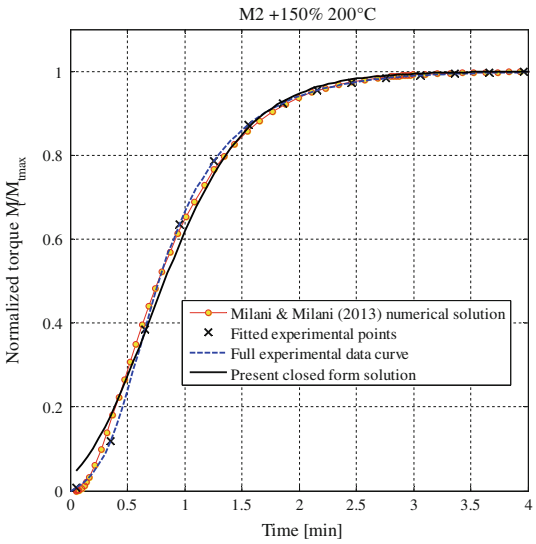

Fig. 19 EPDM vulcanized with M2 curing agent, 200 °C. Comparison among experimental data, previously presented numerical approach and present closed form solution

ical procedure (left) by the author [1], at the three different vulcanization temperatures discussed (a: 160 °C; b: 180 °C; c: 200 °C).

$\Sigma_i |e|$ is the sum of the absolute values $|e|$, being $|e|$ the differences between numerical prediction and experimental normalized torque on a vulcanization instant. The sum is performed on all those experimental points selected within the least squares procedure as target values to fit.

As can be easily shown, such representation may provide an estimate of the convergence velocity and quality of the models from a global point of view. A direct comparison between models and among the three different temperatures is also possible.

From a detailed comparative analysis of the numerical results, the following considerations may be done:

- The convergence rate of the present analytical model is always very high, the model requiring a few iterations to reach the optimal solution. In terms of convergence rate, the present model performs almost always better than [1] numerical approach.
- When dealing with the quality of the solution reached, it can be stated that, at 200 °C, a closer fitting on experimental data is obtained with the present model, whereas at 180 °C, the performance of numerical model [1] is superior. At 160 °C, the present approach generally seems to fit better experimental evidences (even if the curves are still not superimposable in some regions) when compared to the numerical approach proposed in [1]. $\Sigma_i |e|$ at the end of the simulations is similar (compare for instance graphs in Fig. 14), but the shape of the normalized rheometer curve provided by the present approach, see Fig. 8, seems much more realistic and near the experimental one.
- The normalized rheometer curve provided by the present approach does not fit well experimental data near the origin. This behavior was expected, because, see

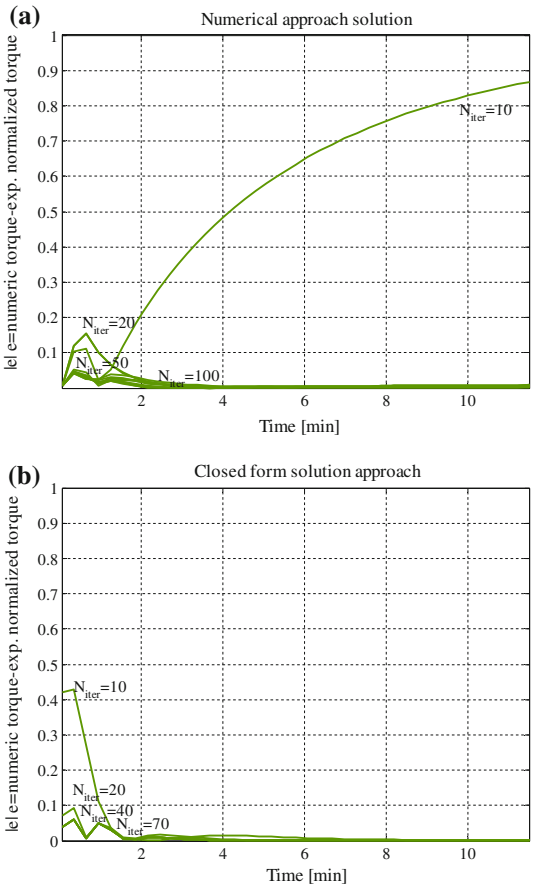

Fig. 20 EPDM vulcanized with M2 curing agent, 200 °C. Absolute error charts at successive iterations. **a** Previously presented numerical approach. **b** Present closed form solution

Eq. (27), the approximate function used for the least squares fitting, Eq. (25), does not pass through the origin of the axes.

4 Conclusions

The numerical model firstly proposed in [1] for the kinetic interpretation of EPDM vulcanized with peroxides has been further developed and refined from a mathematical standpoint and an approximate closed form solution for the second order non-linear and non-homogeneous differential equation representing the crosslink density evolution during curing, 2ODENL Eq. (10), has been proposed. The case of EPDM without reversion has been discussed in detail and the model has been tested on real experimental data. Experimental data to fit are represented either by scaled rheometer curves at fixed temperatures or by scaled crosslink density evaluated experimentally through more sophisticated approaches.

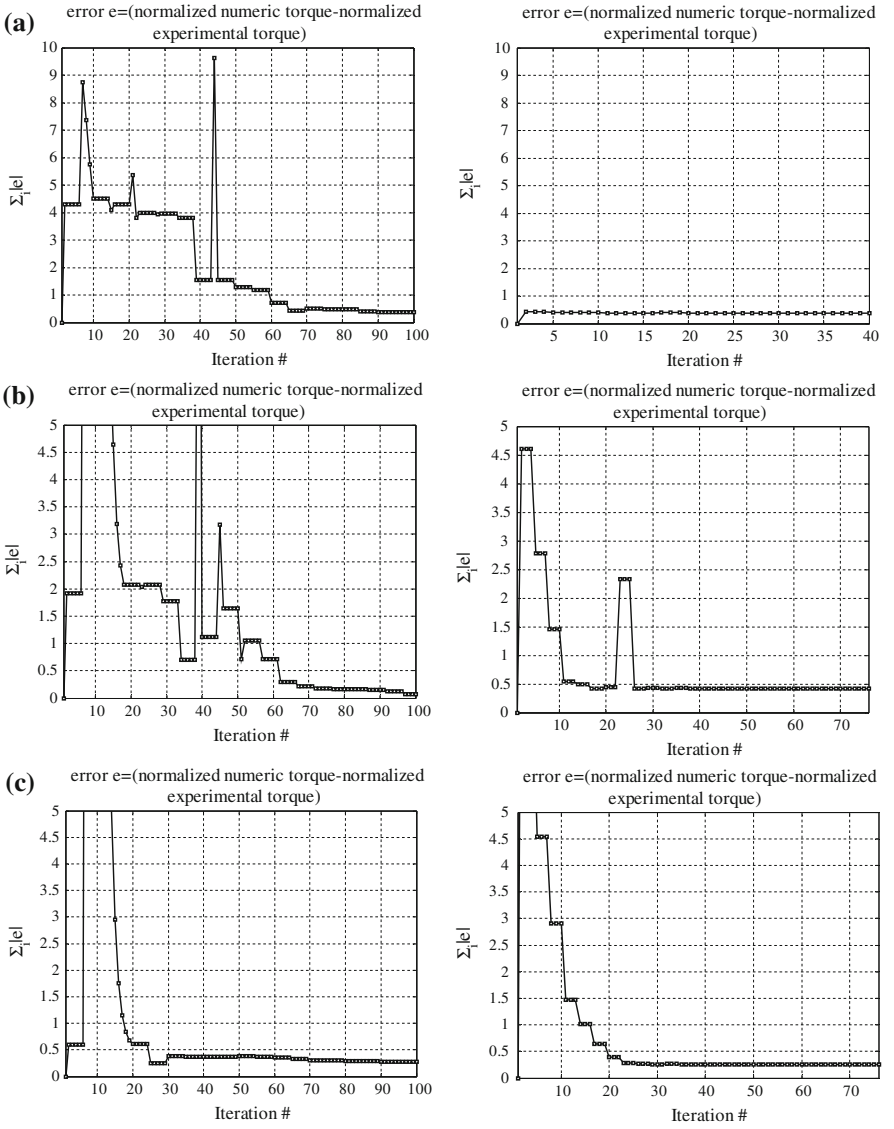

Fig. 21 EPDM vulcanized with M2 curing agent. Convergence of the least squares routine assuming as target the absolute error. *Left*: numerical literature approach. *Right*: present closed form model. **a** 160 °C. **b** 180 °C. **c** 200 °C

When compared with the previous procedure [1], the present approach allows circumventing the utilization of a Runge–Kutta explicit routine to solve 2ODENL differential equation. This is a major improvement, because, in both modes, kinetic constants at the base of the vulcanization process are estimated by means of a non-linear least squares data fitting, which requires having at disposal the solution of 2ODENL

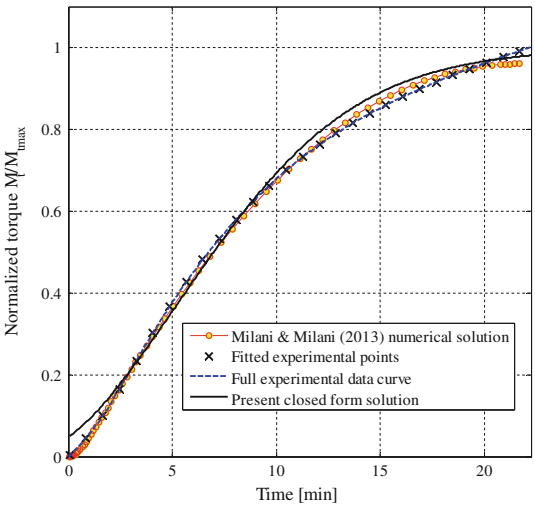

Fig. 22 EPDM vulcanized with Perkadox 14-S, 160 °C. Comparison among experimental data, previously presented numerical approach and present closed form solution

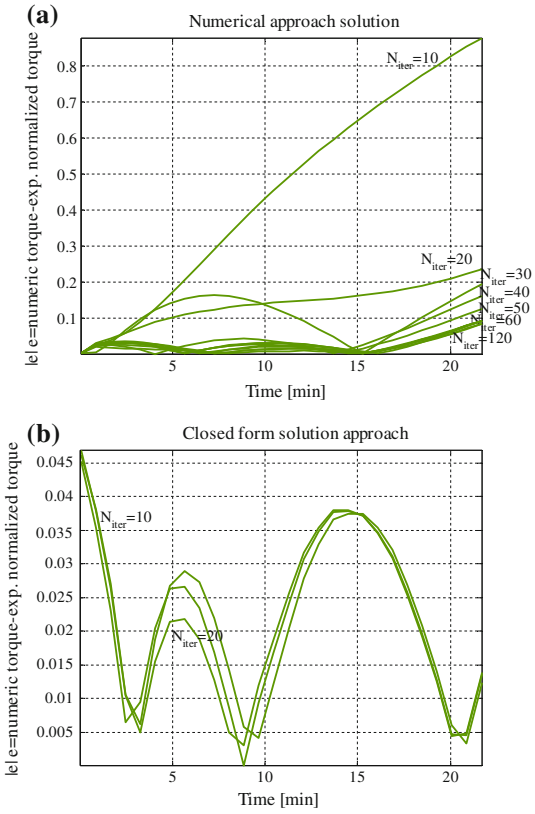

Fig. 23 EPDM vulcanized with Perkadox 14-S, 160 °C. Absolute error charts at successive iterations. **a** Previously presented numerical approach. **b** present closed form solution

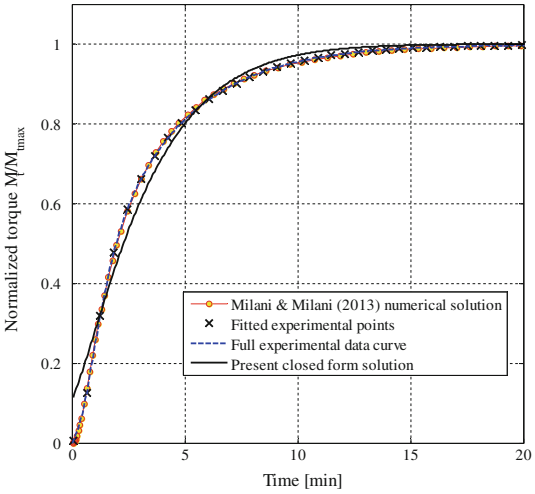

Fig. 24 EPDM vulcanized with Perkadox 14-S, 180 °C. Comparison among experimental data, previously presented numerical approach and present closed form solution

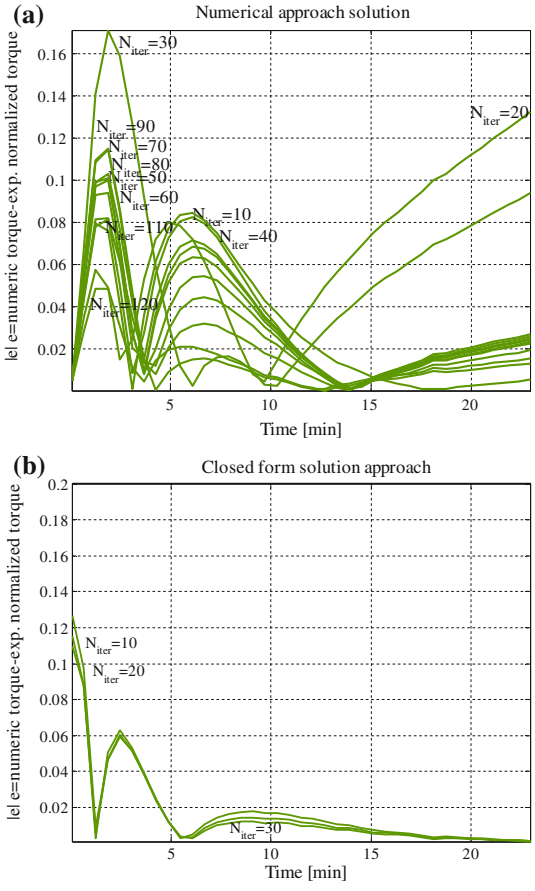

Fig. 25 EPDM vulcanized with Perkadox 14-S, 180 °C. Absolute error charts at successive iterations. **a** Previously presented numerical approach. **b** present closed form solution

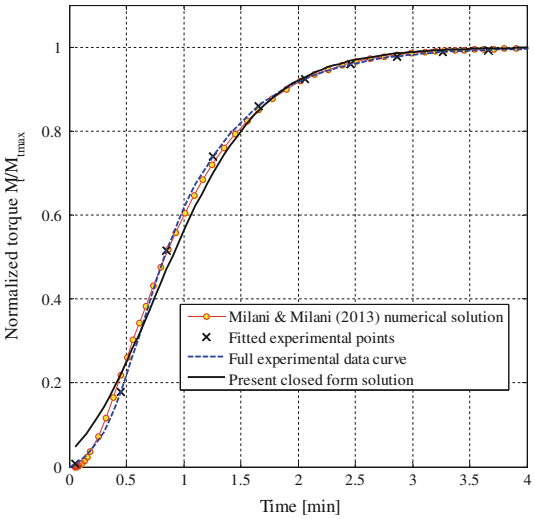

Fig. 26 EPDM vulcanized with Perkadox 14-S, 200 °C. Comparison among experimental data, previously presented numerical approach and present closed form solution

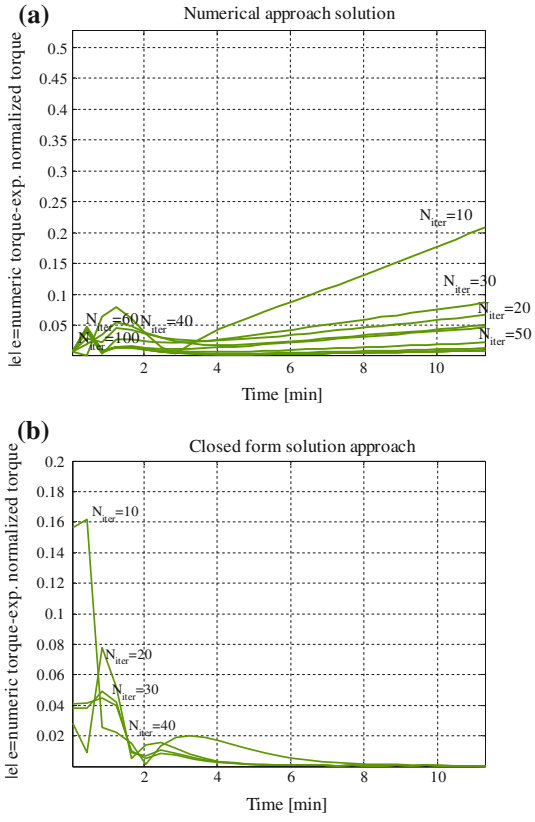

Fig. 27 EPDM vulcanized with with Perkadox 14-S, 200 °C. Absolute error charts at successive iterations. **a** Previously presented numerical approach. **b** Present closed form solution

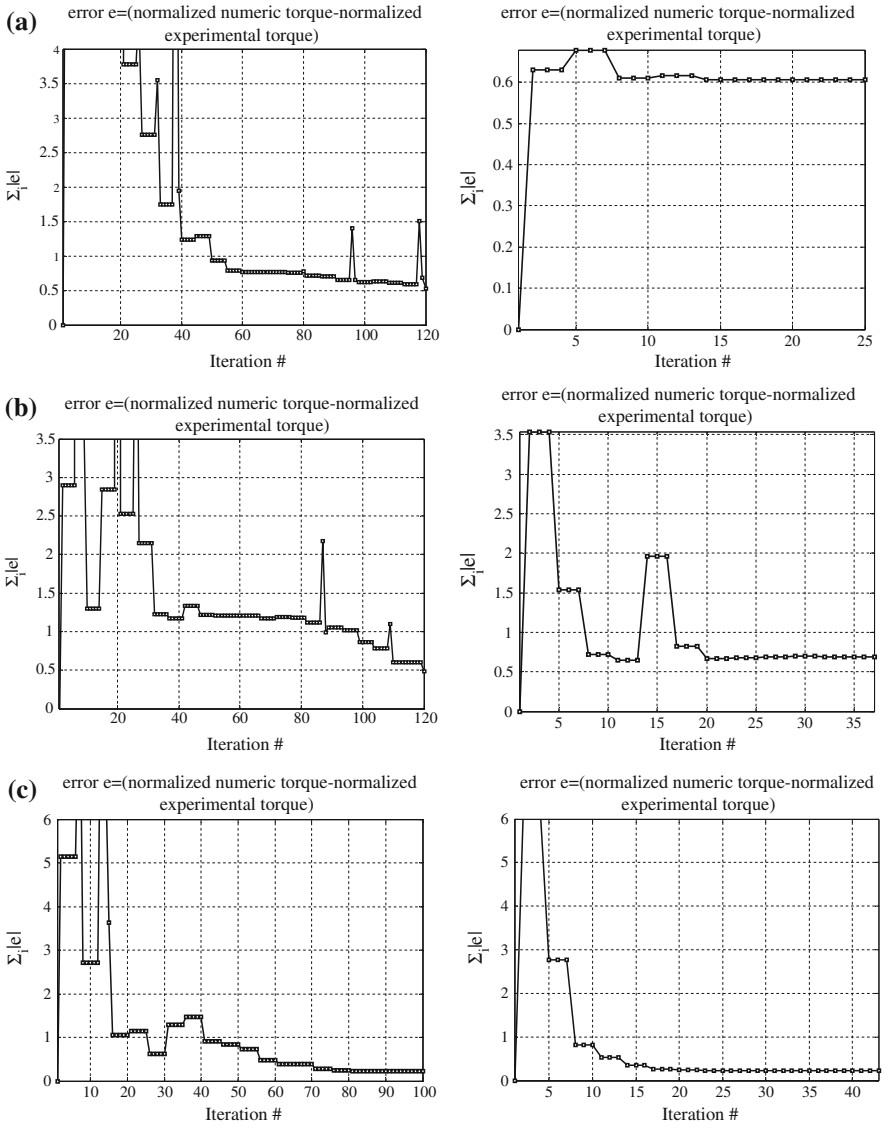

Fig. 28 EPDM vulcanized with Perkadox 14-S. Convergence of the least squares routine assuming as target the absolute error. *Left*: numerical literature approach. *Right*: present closed form model. **a** 160 °C. **b** 180 °C. **c** 200 °C

equation iteration by iteration. As a consequence, the convergence rate of the present approach results much higher.

In order to have an insight into the reliability of the combined numerical/analytical approach proposed, the model has been tested on a single EPDM blend with low unsaturation and crosslinked with three different peroxides at three increasing temperatures. A critical comparison between results obtained with the present and previously pre-

sented numerical approach has been reported, showing how the present closed form solution may fit, in some cases (160 and 200 °C temperatures), experimental data even better than the previously presented numerical procedure.

References

1. G. Milani, F. Milani, J. Math. Chem. **51**(3), 1116–1133 (2013)
2. G. Milani, F. Milani, J. Math. Chem. **47**(1), 229–267 (2010)
3. G. Milani, F. Milani, Comput. Chem. Eng. **32**, 3198–3212 (2008)
4. V. Kosar, Z. Gomzi, Theromochimica Acta **457**, 70–82 (2007)
5. D.C. Seymour, D. Krick, J. Elastomers Plast. **11**, 97–109 (1979)
6. E. Di Giulio, G. Ballini, Kautschuk gummi, kunststoffe **6**(15) (1962)
7. A.Y. Coran, Vulcanization, in *Science and Technology of Rubber, Chapter 7*, ed. by F.R. Eirich (Academic Press, New York, 1978)
8. M. Morton (ed.), *Rubber Technology* (van Nostrand Reinhold, New York, 1981)
9. G. Milani, F. Milani, J. Math. Chem. **48**, 530–557 (2011)
10. G. Milani, F. Milani, J. Appl. Polym. Sci. **124**(1), 311–324 (2012)
11. G. Milani, F. Milani, Comput. Chem. Eng. **43**, 173–190 (2012)
12. W. Hofmann, *Rubber Technology Handbook* (Hanser Publishers, Munich, 1989)
13. G. Milani, F. Milani, Polym. Eng. Sci. **53**(2), 353–369 (2013)
14. M. van Duin, H.G. Dikland, Rubber Chem. Technol. **76**, 132 (2003)
15. M. van Duin, M. Dees, H.G. Dikland, Kautsch. Gummi Kunstst **61**, 233 (2008)
16. M. Dees, M. van Duin, Rubber, World, Aug/Sept (2008)
17. M. van Duin, Kautsch. Gummi Kunstst **55**, 150 (2002)
18. R. Peters, M. van Duin, D. Tonoli, G. Kawakkenbos, Y. Mengerink, R. van Benthem, C. de Koster, P.J. Schoenmakers, S. van der Wal, J. Chromatogr. A **1201**, 151 (2008)
19. R. Orza, P.C.M.M. Magusin, V.M. Litvinov, M. van Duin, M.A.J. Michels, Macromolecules **42**, 8914–8924 (2009)
20. H.G. Dikland, M. van Duin, in *Crosslinking of EPDM and Polydiene Rubbers Studied by Optical Spectroscopy*, eds. by V.M. Litvinov, P.P. De. Spectroscopy of Rubbers and Rubbery Materials (Rapra Technology Ltd. Shawbury, Shrewsbury, Shropshire, 2002), pp. 207
21. M. van Duin, R. Orza, R. Peters, V. Chechik, Macromol. Symp. **291–292**, 66–74 (2010)
22. W.C. Endstra, C.T.J. Wreesman, in *Elastomer Technology Handbook*, ed. by N.P. Cheremisinoff (CRC Press, Boca Raton, 1993), p. 495
23. P. Dluzneski, Rubber Chem. Technol. **74**, 451 (2001)
24. R. Orza, Investigation of peroxide crosslinking of EPDM rubber by solid-state NMR. PhD thesis Technische Universiteit Eindhoven (2008)
25. J.M. Kranenburg, M. van Duin, U.S. Schubert, Screening of EPDM cure states using depth-sensing indentation. Macromol. Chem. Phys. **208**, 915–923 (2007)
26. Matlab User's Guide. http://www.mathworks.com/products/matlab/ (2007)
27. G. Milani, A. Galanti, C. Cardelli, F. Milani, in Peroxide Cross-Linking of EPDM for Medium Voltage Cable Applications: Experimental Insight. *Proceedings of 183rd Technical Meeting Akron*, Ohio Monday, April 22, 2013 –Wednesday, April 24, 2013
28. AkzoNobel. Brochure of organic peroxides. Available at http://www.akzonobel.com/polymer/ (2012)